

1

Supporting Information

2 **Construction of SrTiO₃/Zn_xCd_{1-x}S S-scheme** 3 **heterojunction composites as efficient bifunctional** 4 **photocatalyst for HCHO degradation and hydrogen** 5 **production**

6 *Dianxiang Peng^a, Yanjie Lv^a, Wenxi Zhang^a, Jing Sun^{a,*}, Xiao Li^a, Hongfei Shi^{b,*},*

7 *Zhongmin Su^{a,*}*

8

9 ^a School of Chemical and Environmental Engineering, Jilin Provincial Science and
10 Technology Innovation Centre of Optical Materials and Chemistry, Changchun
11 University of Science and Technology, Jilin Provincial International Joint Research
12 Center of Photo-functional Materials and Chemistry, Changchun, 130022, P. R. China.

13 ^b Institute of Petrochemical Technology, Jilin Institute of Chemical Technology, Jilin,
14 132022, P. R. China.

15 * Corresponding authors

16 Email: Sj-cust@126.com; shihf813@nenu.edu.cn; zmsu@nenu.edu.cn

17

18 **1. Experimental section**

19 ***1.1 Chemicals and materials***

20 Polyvinylpyrrolidone (PVP, $M_w=1300000$, AR), Strontium nitrate ($\text{Sr}(\text{NO}_3)_2$,
21 $>99\%$, AR), Titanium butoxide ($\text{Ti}(\text{OC}_4\text{H}_9)_4$, AR), N,N-Dimethylformamide (DMF,
22 $>99.5\%$, AR), Zinc nitrate ($\text{Zn}(\text{NO}_3)_2 \cdot 6\text{H}_2\text{O}$, $\geq 99.0\%$, AR), Cadmium nitrate
23 ($\text{Cd}(\text{NO}_3)_2 \cdot 4\text{H}_2\text{O}$, $\geq 99.0\%$, AR), Thioacetamide (CH_3CSNH_2 , $>99\%$, AR), Acetate
24 (CH_3COOH , $\geq 99.0\%$, AR), Sodium sulfate (Na_2SO_4 , $\geq 99.0\%$, AR), Potassium chloride
25 (KCl , $>99.5\%$, AR), Sodium sulfide nonahydrate ($\text{Na}_2\text{S} \cdot 9\text{H}_2\text{O}$, $\geq 98\%$, AR), Sodium
26 sulfite (Na_2SO_3 , $\geq 98\%$, AR), Triethanolamine (TEOA, 98% , AR), Isopropyl alcohol
27 (IPA, $\geq 99.5\%$, AR), p-benzoquinone (BQ, AR), Lactic acid ($\text{C}_3\text{H}_6\text{O}_3$, $>99.9\%$, AR),
28 formaldehyde solution (37 wt.% in H_2O , containing 10-15% methanol stabilizer),
29 phenol reagent ($\text{C}_6\text{H}_5\text{O}$, 3-methyl-2-benzothialinone) were obtained from
30 Macklin Biochemical Technology Co., Ltd., China. Potassium ferricyanide
31 ($\text{K}_3\text{Fe}(\text{CN})_6$, $\geq 99.5\%$, AR), Potassium ferrocyanide trihydrate ($\text{K}_4\text{Fe}(\text{CN})_6 \cdot 3\text{H}_2\text{O}$, 99% ,
32 AR) and Barium sulfate (BaSO_4 , 99% , AR), Ethylene glycol ($\text{HOCH}_2\text{CH}_2\text{OH}$, AR),
33 5,5-Dimethyl-1-pyrroline N-oxide (DMPO, 97% , AR), TEMPO ($\text{C}_9\text{H}_{18}\text{NO}$, 98% , AR)
34 were purchased from Aladdin Reagent Co., Ltd., China. Anhydrous ethanol was
35 purchased from Beijing Chemical works. They were used as received without further
36 purification. Deionized water was used throughout the work.

37 ***1.2 Preparation of SrTiO_3 nanofibers***

38 3.4g $\text{Ti}(\text{OC}_4\text{H}_9)_4$ and 2.128 g $\text{Sr}(\text{NO}_3)_2$ were dissolved in N,N-dimethylformamide
39 (40 mL) and acetic acid (10 mL), respectively. Then 4 g of polyvinylpyrrolidone with

40 a molecular weight of 1300000 was added, stirred for 5 h, and the solution was
41 transferred to a 10 mL plastic syringe with **no. 22** stainless steel needle. The feeding
42 speed is $0.8 \text{ mL}\cdot\text{h}^{-1}$, controlled by injection pump, and the high pressure is 15 kV. The
43 distance between the tip of the syringe and the opposite electrode (aluminum foil) is 15
44 cm. The nanofibers were calcined at $1000 \text{ }^\circ\text{C}$ for 6 h at a heating rate of $5 \text{ }^\circ\text{C}\cdot\text{min}^{-1}$ to
45 obtain SrTiO_3 nanofibers.

46 ***1.3 Synthesis of STO/ZCS-x and ZCS***

47 ZCS was prepared by a conventional solvothermal method as follows:
48 $\text{Cd}(\text{NO}_3)_2\cdot 4\text{H}_2\text{O}$ and $\text{Zn}(\text{NO}_3)_2\cdot 6\text{H}_2\text{O}$ were dissolved in 30 mL of deionized water in
49 the ratio of 0.2:0.8. Then 4 mmol of thiourea was added, and the solution was stirred
50 continuously for 1 h and transferred to a 50 mL autoclave and heated continuously at
51 $180 \text{ }^\circ\text{C}$ for 24 h. The resulting sample was collected and washed several times with
52 deionized water and ethanol. Finally, the sample was placed in a vacuum oven and
53 continuously heated at $60 \text{ }^\circ\text{C}$ for 12 h. The sample was recorded as ZCS.

54 The composites were synthesized with mass ratios of $\text{STO}:\text{ZCS}=0.1, 0.3, 0.5, 0.7$
55 and 0.9, respectively. The $\text{STO}/\text{ZCS-x}$ composites were prepared by adding STO at
56 different mass ratios to the above ZCS in a reactor, respectively, with other conditions
57 remaining unchanged.

58 ***1.4 Material characterization***

59 The crystal structures of prepared samples were measured using a Bruker AXS D8
60 Focus X-ray diffractometer (XRD) with $\text{Cu K}\alpha$ radiation ($\lambda= 1.54056 \text{ \AA}$) in the range
61 of $10^\circ\text{-}80^\circ$. Scanning electron microscopy (SEM, JEOL JSM 4800F) coupled with an

62 energy-dispersive X-ray (EDX) spectrometer was employed to investigate the
63 morphology of the photocatalysts, and the transmission electron microscopy (TEM)
64 and HRTEM images were taken on a JEM-2100F microscope operated at 200 kV. The
65 Brunauer-Emmett-Teller (BET) specific surface areas were performed on a
66 Micromeritics ASAP-2460 Automatic specific surface area and porous physical
67 adsorption analyzer. The UV-Vis diffuse reflection spectra (DRS) were obtained with
68 a Shimadzu UV-2650 UV-vis spectrophotometer with wavelength range of 200-800
69 nm with BaSO₄ as a reference. Typically, the band gap energy (E_g) of a
70 semiconductor can be determined using the Kubelka-Munk function: $(\alpha h\nu)^{0.5}$
71 $= A(h\nu - E_g)$ (A is the constant; $h\nu$ is the photon energy; α is the absorptivity index; h is
72 the planck's constant; ν is the incident photon frequency; E_g is the bandgap of
73 semiconductor). The photoluminescence (PL) spectra were measured by a Perkin-
74 Elmer LS55 fluorescence spectrophotometer with excitation wavelength of 705 nm at
75 room temperature. Electron spin-resonance spectroscopy (ESR) was collected on a
76 magnettech MS-5000 instrument. The electrochemical measurements were
77 implemented on a CHI 760E electrochemical workstation (Shanghai, Chenhua).

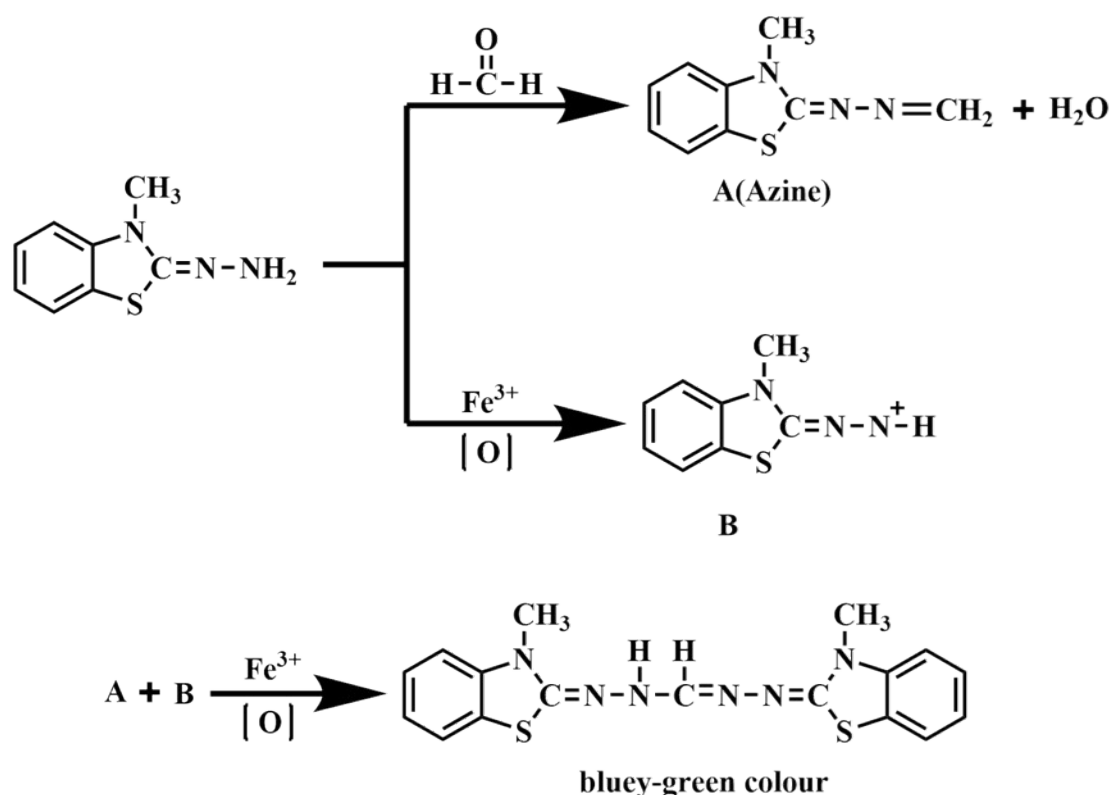
78 ***1.5 Photocatalytic HCHO degradation test***

79 The photocatalytic performances of catalysts were evaluated by the
80 photodegradation of HCHO. A 300 W Xenon lamp with 400 nm cut-off filter was used
81 as visible light source and a 50 mL stainless-steel batch reactor was employed as the
82 reactor (CEL-GPR100, AULTT, China). The photocatalyst (20 mg) were dispersed in
83 5 mL ethanol and ultrasonicated for 10 minutes. Then, the mixed liquid is loaded on

84 the quartz plate, and the catalyst is loaded on the dishes after heated at 60 °C in an oven
85 to completely remove the ethanol. Then, the quartz plate with catalyst was placed into
86 the closed photocatalytic reactor. 37% formalin solution was used as the gas source of
87 HCHO. A certain volume of formalin solution is directly dropped into the glass reagent
88 bottle in the reactor, then the upper quartz window is sealed, and then the formalin
89 solution was heated by infrared light to accelerate evaporation. The water vapor or N₂
90 were injected into the reactor through a gas distribution system (CEL-GPPCN, AULTT,
91 China). The reactor temperature can be control by external circulation heating and
92 cooling device. The gas circulation pump was used to promote the diffusion of HCHO
93 gas. Before illumination, the HCHO gas was diffused in the dark for 20 min to achieve
94 the uniform distribution of HCHO gas and to ensure the adsorption-desorption
95 equilibrium between HCHO and catalyst powder. When the balance of gas desorption
96 is reached, the xenon lamp is turned on and the irradiation begins.

97 The change of HCHO concentration was detected by spectrophotometry. Every 10
98 minutes, 5 mL of gas was extracted by syringe and quickly injected into the brown glass
99 reagent bottle with rubber stopper. The bottle was filled with phenol reagent (MBTH)
100 chromogenic solution in advance. The brown bottle was shaken sufficiently to make
101 the HCHO completely dissolved in the solution, then it was placed in a 40 °C water
102 bath for 10 minutes, then NH₄Fe(SO₄)₂ was added, and then it was shaken sufficiently
103 and placed in a 40 °C water bath for 10 minutes, and the color of solution gradually
104 turned blue-green. The formed blue-green solution has characteristic absorption peak
105 at 630 nm. The change trend of HCHO relative content was determined according to

106 the intensity of the absorption peak at 630 nm. According to the formulas of $A=(1-$
 107 $C/C_0)\times 100\%$ to calculate the removal rate and $k = -\ln(C/C_0)$ to calculate the reaction
 108 rate constant of the pollutants (A is the removal rate; k is the reaction rate constant; C_0
 109 is the concentration of pollutants before illumination. C is the concentration of
 110 pollutants after light exposure).



111

112 **Scheme. S1.** Color reaction of formaldehyde with phenol reagent.

113 As shown in **Scheme. S1**, the phenol reagent reacts with formaldehyde to form
 114 azine. The azine is oxidized by $\text{NH}_4\text{Fe}(\text{SO}_4)_2$ to blue-green dichromate formaldehyde-
 115 3-methyl-2-benzothiazolone hydrazone in acidic solution. The concentration of
 116 formaldehyde can be determined by measuring its absorbance with a
 117 spectrophotometer.

118 **1.6 Photocatalytic hydrogen evolution test**

119 The photocatalytic water-splitting experiments were performed in a Pyrex reaction
120 cell connected to a closed gas circulation and evacuation system (CEL-SPH₂N,
121 CEAULIGHT, China). 50 mg of as-prepared catalysts were dispersed in a 60 mL
122 aqueous solution containing 0.35 mol/L Na₂S and 0.35 mol/L Na₂SO₃. After being
123 purged with argon to thoroughly remove dissolved air, the solution was irradiated by a
124 300 W Xe lamp (CEL-HXF300, AULIGHT, Beijing) equipped with an uvcut-420 filter.
125 The photoreactor was equipped with a cooling jacket circulating water flow to maintain
126 a constant temperature (5 °C). The evolved amounts of H₂ were analyzed by a gas
127 chromatograph (GC-7920, N₂ as carrier gas). The stability test was carried out every 5
128 h and repeated for 5 times. The apparent quantum efficiency (AQE) test for H₂
129 evolution was performed by equipping the 300 Xe lamp with 420 nm band-pass filter
130 to provide the monochromic light. The number of incident photons was determined by
131 an irradiatometer (CEL-NP2000-2, Aulight Corporation, China). The AQE value was
132 calculated from the following equation:

$$133 \text{ AQE} = \frac{\text{Number of reacted electrons}}{\text{Number of incident photons}} \times 100\%$$
$$134 \frac{2 \times n_{\text{H}_2}}{\frac{P \times t \times \lambda}{h \times c}} \times 100\%$$

135 in which n_{H_2} represents the evolved number of H₂ molecules; $t=1.8 \times 10^4$ s is the
136 radiating time; P is the calculated light power; h (6.63×10^{-34} J·s) means the Planck
137 constant; the wavelength of incident light is denoted as λ , and 3.0×10^8 m·s⁻¹ is pointed
138 to the value of c for the light rate.

139 ***1.7 Active species trapping experiment and ESR measurements***

140 The free radical-trapping experiments were carried out to explore the degradation

141 mechanism. P-benzoquinone (BQ), triethanolamine (TEOA) and isopropanol (IPA)
142 were used as the $\cdot\text{O}_2^-$, h^+ and $\cdot\text{OH}$ radicals scavengers, respectively. The trapping agents
143 and photocatalyst were dispersed in 30 mL ethanol and ultrasonicated for 30 minutes.
144 Then, the mixed liquid is loaded on the dishes, and the catalyst and capturing agent are
145 loaded on the dishes after heated at 60 °C in an oven to completely remove the ethanol.
146

147 The ESR spectra techniques with DMPO and TEMPO were performed to further
148 confirm radical generation in the photocatalytic reaction system under visible-light
149 irradiation. The electron spin resonance spectra (ESR) measurement processes: 2 mg
150 composite sample was dispersed in 1 mL distilled water, then took out 50 μL above-
151 mentioned dispersion liquid and mixed with 50 μL of spin-trapped reagents DMPO and
152 TEMPO. The sample was subsequently transferred to an ESR flat cell and passed into
153 the optical path, then spectra were taken by a magnettech MS-5000 instrument
154 spectrometer during the process of visible-light irradiation.

155 ***1.8 Electrochemical measurements***

156 The electrochemical characterizations were conducted with a CHI760E
157 electrochemical workstation (Shanghai Chen Hua Instrument Co., Ltd., China) with a
158 conventional three-electrode configuration in a quartz cell. For photoelectrochemical
159 measurement, an Ag/AgCl electrode and Pt foil were used as the reference electrode
160 and counter electrode, respectively. A 0.5 M Na_2SO_4 aqueous solution was used as
161 electrolyte. A 300 W Xe lamp was employed to provide light source. Typically, the
162 working electrodes were prepared as follows: 20 mg of various catalyst was dispersed

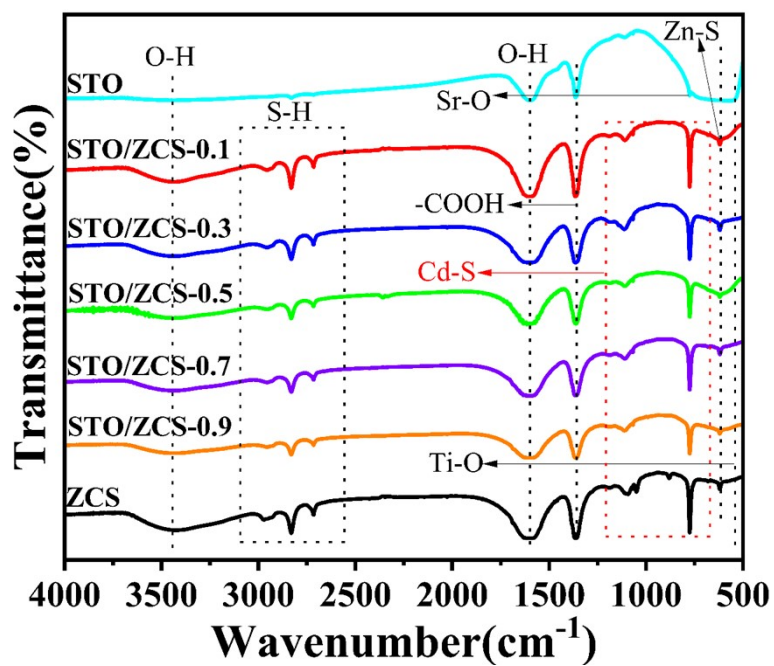
163 into 3 mL of ethanol with sonication for 20 min. Then, 0.5 mL of the above solution
164 was uniformly dropped onto a 1×3 cm² FTO glass substrate (an active area of ca. 2
165 cm²). Finally, the as-prepared electrodes were dried at 70 °C for 4 h to obtain the
166 working electrodes.

167 The electrochemical impedance spectroscopy (EIS) data was collected in 0.1 M
168 KCl solution containing 5 mM Fe(CN)₆^{3-/4-} with a frequency range from 0.01 Hz to 10
169 kHz at 0.1 V. And the equivalent circuit was obtained using Zview software. The Mott-
170 Schottky test was carried out with a standard three-electrode system using the prepared
171 glass electrode as the working electrode, a Pt wire as a counter electrode, Hg/Hg₂Cl₂
172 electrode as a reference electrode, respectively. A 0.5 M Na₂SO₄ solution was applied
173 as the electrolyte. Mott-Schottky plots were measured at a fixed frequency of 2000,
174 2500 and 3000 Hz and an amplitude of 50 mV without light illumination. The linear
175 sweep voltammetry (LSV) data was recorded at a potential scan from 0.2 V to -1.4 V
176 at a sampling interval of 0.001 V under a 300 W xenon lamp illumination. The cyclic
177 voltammetry (CV) curves were collected at different scan rate from 5–140 mV·s⁻¹.

178 ***1.9 In situ XPS measurements***

179 In situ X-ray Photoelectron Spectroscopy (XPS) Testing Parameters:
180 Manufacturer: Thermo Fisher Scientific, United States; Model: Escalab 250Xi;
181 Excitation Source: Aluminum K-alpha (Al Kα); Analysis Area: 500 micrometers (μm);
182 Testing Pressure: Lower than 10⁻⁷ Pascals (Pa). The XPS analyses were first conducted
183 in complete darkness. After this, the Xe-light was switched on for in-situ irradiation,
184 and the XPS analyses were repeated after 2 minutes.

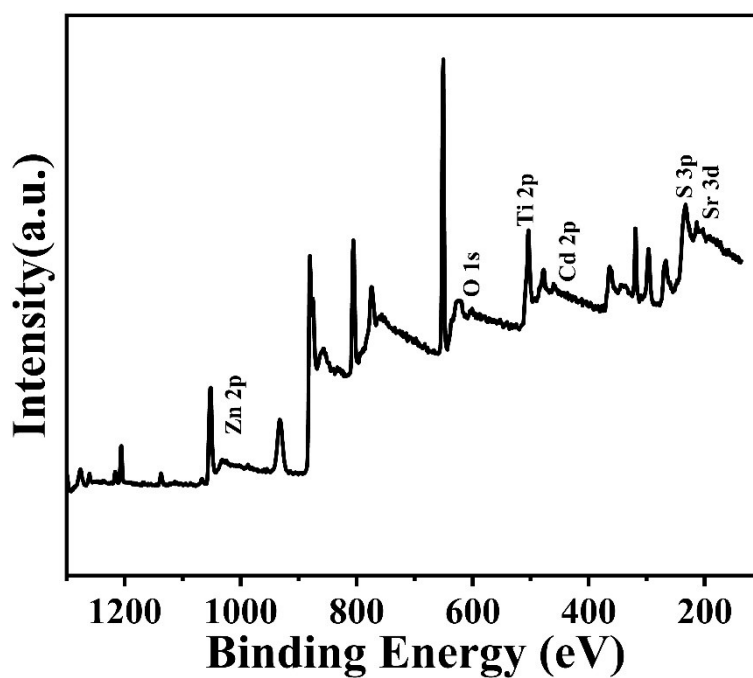
185 **2. Supplementary Figures and Tables**



186

187 **Fig. S1.** FT-IR spectra of various samples.

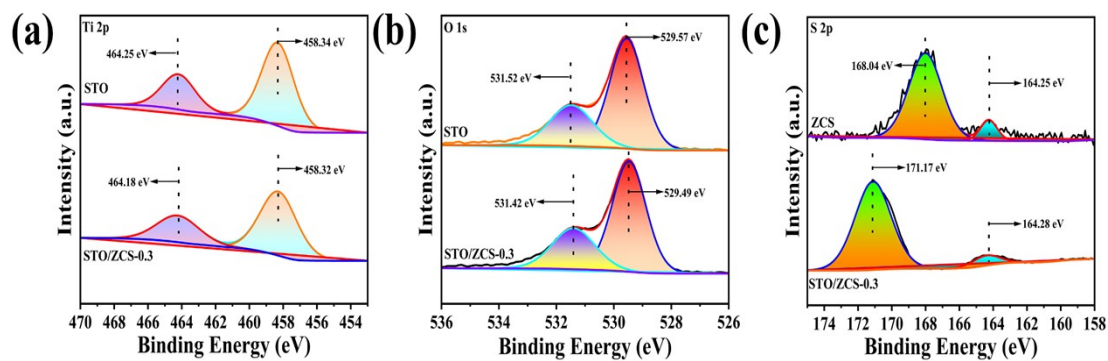
188



189

190 **Fig. S2.** High-resolution spectra of Full survey.

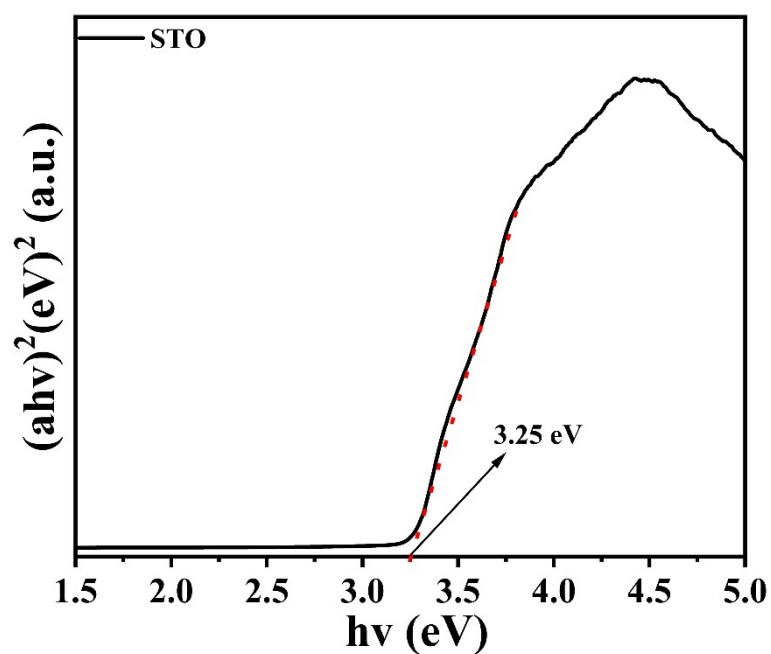
191



192

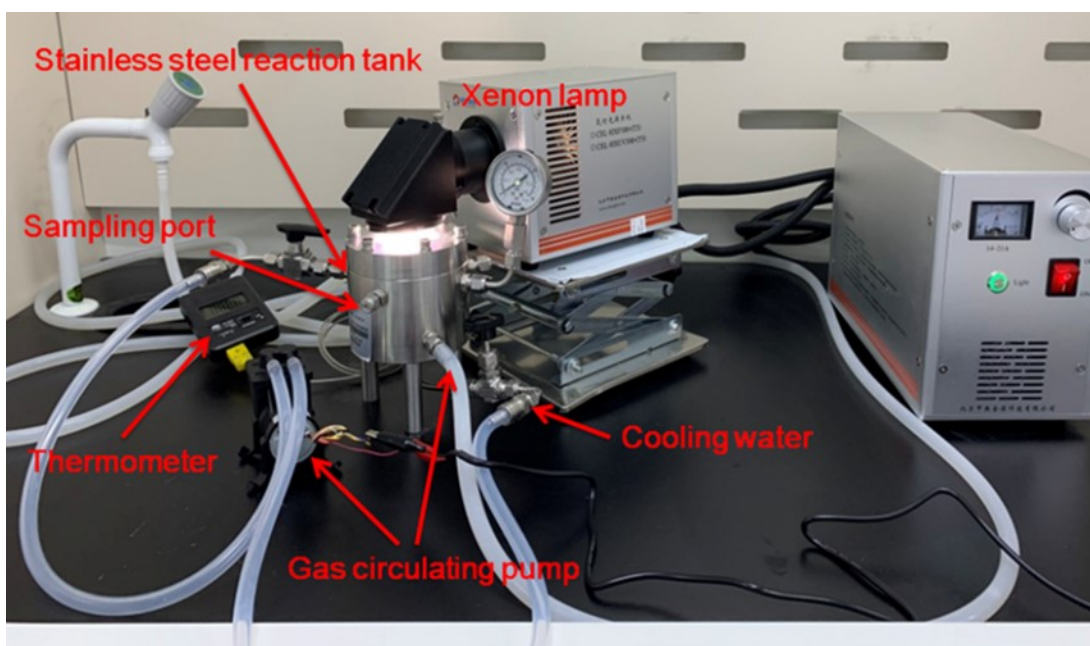
193 **Fig. S3.** High-resolution spectra of (a) Ti 2p, (b) O 1s; (c) S 2p XPS data for STO,

194 ZCS, STO/ZCS-0.3.



195

196 **Fig. S4.** Band gap of STO.

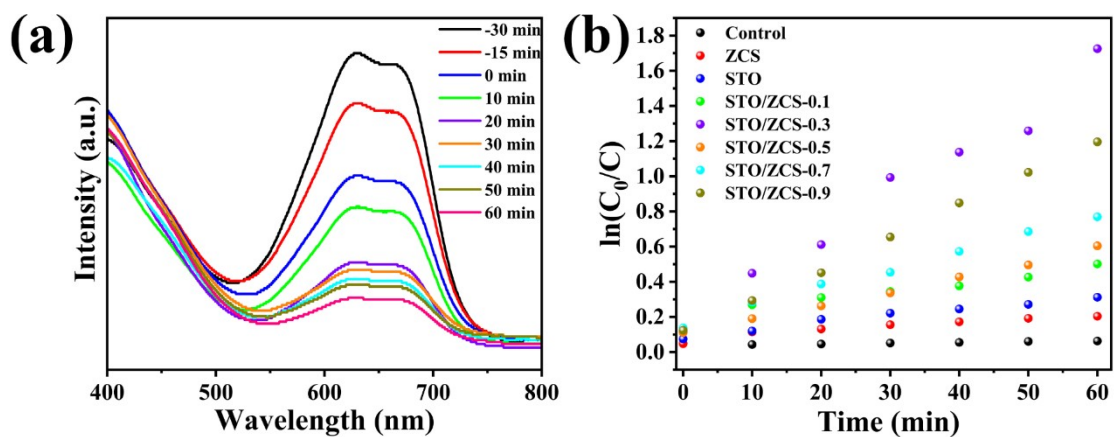


197

198 **Fig. S5.** Stainless steel closed gas phase photocatalytic reactor.

199 **Fig. S5** shows the photocatalytic setup. The catalytic equipment includes xenon
200 lamp, stainless steel reaction tank, thermometer and gas circulation pump. The upper
201 part of the reaction tank can be opened. After opening, the catalyst and formalin
202 solution are added to the reaction tank respectively, and then covered with quartz glass
203 for sealing. There are two groups of valves on the side of the reaction tank, which are
204 connected to cooling water and gas circulating pump respectively. There is a sampling
205 port on the side of the reaction tank, which is closed by a rubber plug. The gas in the
206 reaction tank can be extracted through a syringe for color reaction and absorbance
207 measurement.

208

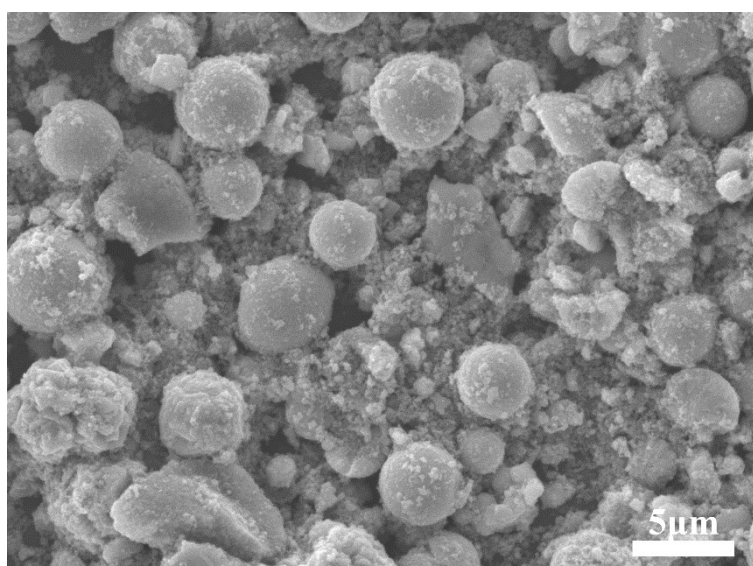


209

210 **Fig. S6.** (a) The spectral changes of HCHO after color reaction with phenol reagent;

211 (b) Relationship curve between $\ln(C/C_0)$ and time.

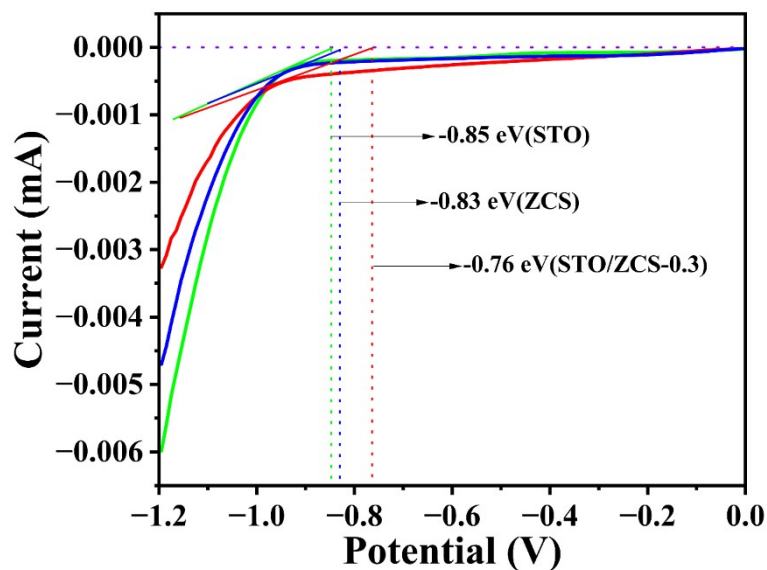
212



213

214 **Fig. S7.** Data comparisons of SEM by STO/ZCS-0.3 after HCHO degradation.

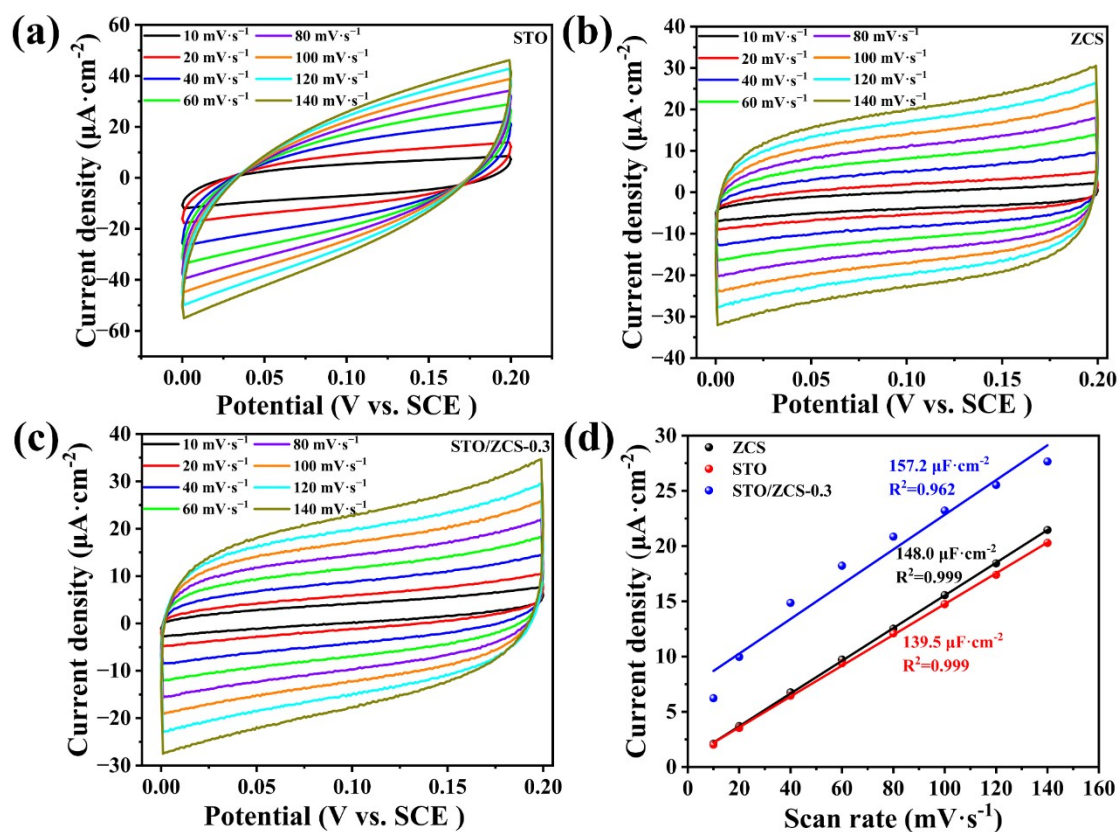
215



216

217 **Fig. S8.** LSV curves of the photocatalysts.

218

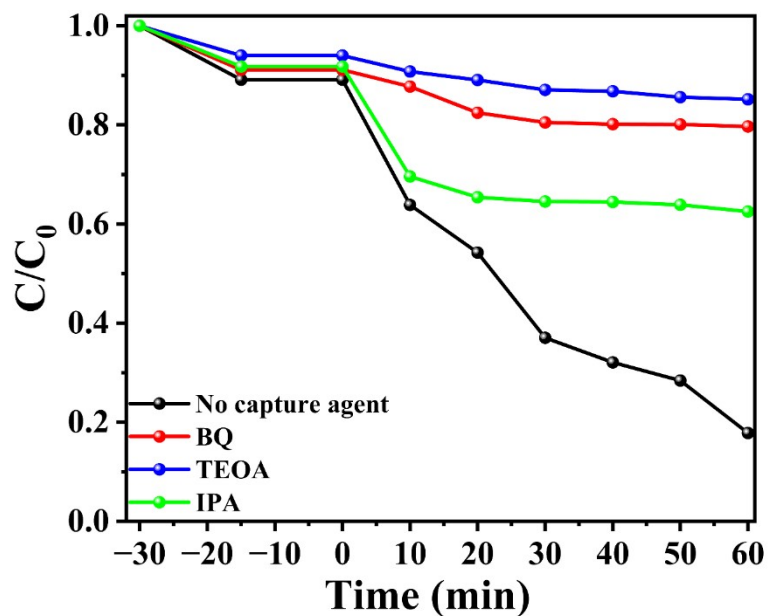


219

220 **Fig. S9.** CV curves of (a) STO, (b) ZCS, and (c) STO/ZCS-0.3 at different scan rates;

221 (d) Fitting curves of the relationship between scan rate and current density.

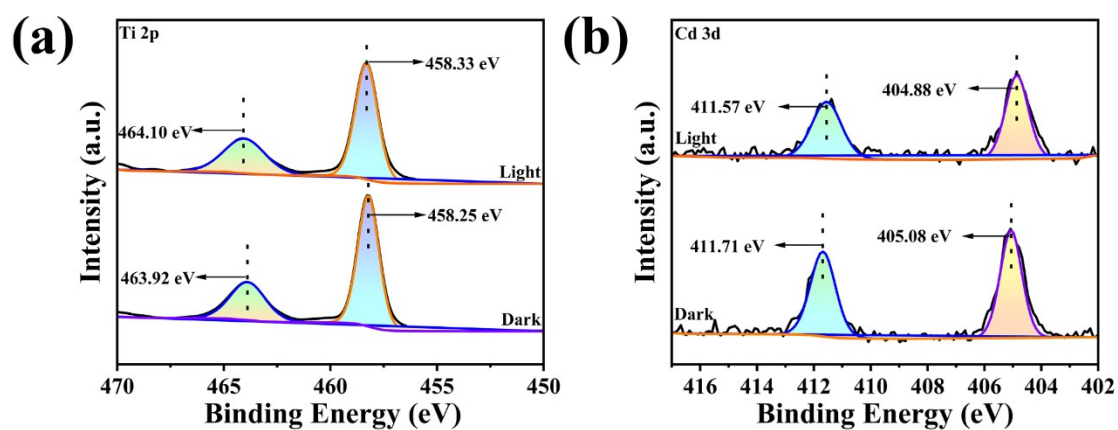
222



223

224 **Fig. S10.** Quenching tests for HCHO removal.

225



226

227 **Fig. S11.** The in situ irradiated XPS spectra of STO/ZCS in darkness and under light

228 illumination: (a) Ti 2p; (b) Cd 3d.

229

230

231

232

233

234

235 **Table S1.** The comparison of photocatalytic HCHO removal of STO/ZCS-0.3 with

236 various photocatalysts.

Photocatalyst	Time (min)	Removal (%)	Light source	Reference
$\text{Bi}_4\text{O}_5\text{Br}_2/\text{Bi-MOF}$	60	90.1	300 W Xe lamp	1
$\text{g-C}_3\text{N}_4/\alpha\text{-Fe}_2\text{O}_3$	120	63.04	300 W Xe lamp	2
$\text{SrTiO}_3/\text{SrCO}_3$	30	40.3	350 W Xe lamp	3
$\text{Ag}/\text{BiOBr}/\text{rGO}$	60	69	300 W Xe lamp	4
$\text{g-C}_3\text{N}_4\text{-TiO}_2/\text{waste zeolites}$	30	58.6	10 W LED lamp	5
BiOI@Carbon	40	73	300 W Xe lamp	6
$\text{MIL-68(In)-NH}_2/\text{GO}$	60	77	50 W LED lamp	7
BiOI-RGGMs	120	87.46	300 W Xe lamp	8
$\text{ZnMn}_2\text{O}_4\text{-BiVO}_4$	240	66	Light source- fluorescent lamp (20 W)	9

PMo ₁₂ /MgIn ₂ S ₄	60	64.81	300 W Xe lamp	10
STO/ZCS-0.3	60	82.2	300 W Xe lamp; λ > 420 nm	This work

- 237 [1] Y. S. Li, D. M. Han and Z. H. Wang, Double-Solvent-Induced Derivatization of
238 Bi-MOF to Vacancy-Rich Bi₄O₅Br₂: Toward Efficient Photocatalytic Degradation of
239 Ciprofloxacin in Water and HCHO Gas. ACS Appl. Mater. Interfaces., 2024, 16,
240 7080–7096.
- 241 [2] Y. D. Wang, N. Zhang and C. Q. Zhang, Utilising bauxite residue (red mud) to
242 construct Z-type heterojunction for formaldehyde degradation. J. Clean. Prod., 2024,
243 444, 141280.
- 244 [3] S. W. Han, X. W. Li and Y. Tan, In-situ self-sacrificed fabrication of insulator-
245 based SrTiO₃/SrCO₃ heterojunction interface for gaseous HCHO and NO
246 photocatalytic degradation, Appl. Surf. Sci., 2023, 612, 155806.
- 247 [4] G. Yan, L. J. Zhou and B. L. Yang, Ternary Ag/BiOBr/rGO nanoflower composite
248 as a high-efficiency photocatalyst for formaldehyde and rhodamine B degradation.
249 New. J. Chem., 2023, 47, 12248-12258.
- 250 [5] S. H. Liu and W. X. Lin, A simple method to prepare g-C₃N₄-TiO₂/waste zeolites
251 as visible-light-responsive photocatalytic coatings for degradation of indoor
252 formaldehyde, J. Hazard. Mater., 2019, 368, 468-476.
- 253 [6] G. Yan, R. H. He and X. Z. Cao, Study on photocatalytic degradation of
254 formaldehyde and rhodamine b by BiOI@Carbon sphere core-shell nanostructures
255 composite photocatalyst. Inorg. Chem. Commun., 2024, 164, 112410.
- 256 [7] Y. Y. Yao, J. Yuan and Z. C. Wang, Efficient visible-light-driven photocatalytic
257 degradation of indoor formaldehyde using an indium-based MOF/graphene oxide
258 composite. J. Photoch. Photobio. A., 2025, 460, 116102.
- 259 [8] P. Lu, N. Zhang and Y. Wang, Synthesis of BiOX-Red Mud/Granulated Blast
260 Furnace Slag Geopolymer Microspheres for Photocatalytic Degradation of

261 Formaldehyde. *Materials*, 2024, 17, 1585.

262 [9] P. Y. Wua, S. Attarde and C. C. Lu, ZnMn₂O₄-BiVO₄ as Photocatalyst for
263 Degradation of Gaseous HCHO Using Daylight. *ChemistrySelect*, 2024, 9,
264 e202401501.

265 [10]A. Rong, H. F, Shi and Q. Zhao, Boosted photocatalytic performance of hydrogen
266 evolution and formaldehyde degradation with a S-scheme PMo₁₂/MgIn₂S₄
267 heterojunction, *Sep. Purif. Technol.*, 2024, 348, 127782.

268

269 [11]K. Wang, X. J. Yu and Z. B. Liu, Reconstruction of interface band structure to
270 construct SrTiO₃/BiOBr Z-scheme heterojunction for efficient oxytetracycline
271 degradation and hydrogen recovery. *Appl. Surf. Sci.*, 2024, 684, 161977.

272 [12]Q. Zhou, W. Y. Ren and Y. Y. Wang, Synthesis and visible-light photocatalytic
273 performance of Ce-BiVO₄/SrTiO₃ Z-scheme heterojunction for H₂ production and
274 organic pollutant degradation. *J. Alloy. Compd.*, 2024, 177817.

275 [13]X. Y. Ye, H. Y. Zhong and Y. M. Zhang, Ti₃C₂ MXene cocatalyst supported
276 Ti₃C₂/SrTiO₃/g-C₃N₄ heterojunctions with efficient electron transfer for photocatalytic
277 H₂ production. *Crystengcomm*, 2024, 26(38), 5440-5451.

278 [14]H. M. Cheng, Z. M. Bai and R. X. Cong, SrTiO₃: Al/Cd_{0.6}Zn_{0.4}S Type-II
279 Heterojunction Photocatalysts for Efficient Solar Water Splitting. *J. Phys. Chem. C.*,
280 2024, 128(30), 12427–12436.

281 [15]J. T. Niu and Q. Hu, Facile Fabrication of SrTiO₃/In₂O₃ on Carbon Fibers via a
282 Self-Assembly Strategy for Enhanced Photocatalytic Hydrogen Production.
283 *Sustainability-Basel*, 2024, 16(10), 3988.

284 [16]S. Yousefi and A. Sadeghzadeh-Attar, Coupling effect of Fe-doped Co₃O₄
285 nanoparticles with SrTiO₃ nanotubes on the high-efficiency photocatalytic activities of
286 basic violet 16 dye degradation and H₂ evolution. *Inorg. Chem. Commun.*, 2024, 162,
287 112273.

288 [17]K. J. Gao, K. Li and J. K. Pan, Fabrication of a dual p-n heterojunction consisted
289 of NiCo₂O₄/NiO/Al-doped SrTiO₃ for boosted photocatalytic overall water splitting.
290 *Appl. Surf. Sci.*, 2024, 644, 158794.

291 [18]L. Tian, X. J. Guan and Y. C. Dong, Improved overall water splitting for
 292 hydrogen production on aluminium-doped SrTiO₃ photocatalyst via tuned surface band
 293 bending. *Environ. Chem. Lett.*, 2023, 21(3), 1257-1264.

294 [19]Q. Hu, J. T. Niu and K. Q. Zhang, One-Dimensional CdS/SrTiO₃/Carbon Fiber
 295 Core–Shell Photocatalysts for Enhanced Photocatalytic Hydrogen Evolution. *Coatings*,
 296 2022, 12(9), 1235.

297 [20]T. Ahamad and S. M. Alshehri, Fabrication of Ag@SrTiO₃/g-C₃N₄
 298 heterojunctions for H₂ production and the degradation of pesticides under visible light.
 299 *Sep. Purif. Technol.*, 2022, 297, 121431.

300

301

302 **Table S2.** The comparison of photocatalytic H₂-production activity of STO/ZCS-0.3

303 with previous literatures.

Catalyst	Sacrificial reagents and concentration	Dosage (mg)	Hydrogen evolution rate (μmol·g ⁻¹ ·h ⁻¹)	Light source	Reference
SrTiO ₃ /BiOBr	40 mg/L TEOA	1 mg/mL	65.4	250 W Xe lamp	11
Ce-BiVO ₄ /SrTiO ₃	100 mL H ₂ O	50 mg	154.26	-	12
Ti ₃ C ₂ /SrTiO ₃ /g-C ₃ N ₄	20 mL CH ₃ OH	20 mg	1733.13	300 W Xe lamp	13
SrTiO ₃ :Al/Cd _{0.6} Zn _{0.4} S	0.25 M Na ₂ S+0.35 M Na ₂ SO ₃	200 mg	3550	300 W Xe lamp	14
SrTiO ₃ /In ₂ O ₃	0.25 M Na ₂ S+0.35 M Na ₂ SO ₃	100 mg	320.71	300 W Xe lamp	15
SrTiO ₃ /Fe:Co ₃ O ₄	10 mL CH ₃ OH	50 mg	1718	400 W Xe lamp	16

NiCo ₂ O ₄ /NiO/ Al: SrTiO ₃	100 mL H ₂ O	15 mg	1740	300 W Xe lamp	17
Al-doped SrTiO ₃	100 mL H ₂ O	20 mg	4100	300 W Xe lamp	18
CdS/SrTiO ₃ /Ca Carbon Fiber	0.35 M Na ₂ S+0.25 M Na ₂ SO ₃	100 mg	577.39	300 W Xe lamp	19
Ag@SrTiO ₃ /g- C ₃ N ₄	5 mg/L Dicofol	50 mg	645.62	300 W Xe lamp	20
STO/ZCS-0.3	0.35 M Na₂S+0.35 M Na₂SO₃	50 mg	2566.15	300 W Xe lamp; λ > 420 nm	This work